Sixth International Symposium on Turbulence and Shear Flow Phenomena
Seoul, Korea, 22-24 June 2009

EXPERIMENTAL AND MODELLING STUDY OF TURBULENCE UNDER ZERO-MEAN-FLOW CONDITIONS

Emir Sirbubalo, Matthias Kinzel, Suad Jakirlić and Cameron Tropea
Department of Fluid Mechanics and Aerodynamics (SLA),
Technische Universität Darmstadt
Petersenstr. 30, 64287 Darmstadt, Germany
{esirbubalo,m.kinzel,s.jakirlic,ctropea}@sla.tu-darmstadt.de

ABSTRACT

Symmetry analysis of the evolution equation for the two-point correlation tensor $R_{ij}\left(x_k, r_l, t\right)$ in the case of planar generation of turbulence in an otherwise calm semi-infinite body of fluid has revealed some interesting solutions concerning the statistical properties of turbulence and how they develop with distance from the generation source. The first solution concerns the classical case of shear-free turbulent diffusion. Here, the turbulent kinetic energy is distributed according to a power law x^{-n} where n is a constant larger than one, and x is the normal distance to the forcing plane. The integral length scales of turbulence increase linearly with x. A second case is considered when the symmetry of scaling of space is broken by introducing confinement to the flow. The turbulent kinetic energy decays with x as $\exp\left(-x\right)$ and the integral length scales remain constant along x. The purpose of the present work is to investigate the propagation of the interface separating the turbulent from the non-turbulent (turbulent/non-turbulent interface, TNTI) flow regions, for the two cases using particle image velocimetry (PIV) and large eddy simulation (LES).

INTRODUCTION

The problem considered in this work is the propagation of turbulent motions from a planar source of energy into an infinite body of fluid without mean velocity gradients. At the level of the one-point, second-order velocity moments this condition corresponds to a zero mean rate of production of turbulent stresses from their governing equations. The relevance of this case has been recognized in several contexts, e.g. turbulence at the air-water interface, determination of the empirical constants in the two-equation $k-\epsilon$-type models, in atmospheric and geophysical turbulence investigations, to name a few (e.g. Lele, 1985, Hopfinger et al., 1982).

The fluid motion in this setting can be described as partially turbulent. It gives rise to the concept of the TNTI which separates the vortical, turbulent region from the essentially irrotational non-turbulent region, which is, however, not completely void of the velocity fluctuations. The TNTI is a thin, spatially and temporaly irregular layer, contorted on a range of length scales. It propagates into the turbulent region by the entrainment process. It has been established that the prevailing mechanism responsible for the entrainment is the small-scale "nibbling", as opposed to the large-scale "engulfment" process (Westerweel et al., 2005).

Oberlack and Guenther (2003) have applied the method of symmetry analysis of differential equations to the equations governing the two-point correlation of velocity, defined by $R_{ij}\left(x_k, r_l, t\right) \equiv \left\langle u_i\left(x_k, t\right) u_j\left(x_k + r_l, t\right)\right\rangle$. The analysis has been carried out by utilizing an asymptotic expansion of R_{ij} in the r-space, thereby avoiding the influence of the viscosity on the large scales and recovering an additional scaling symmetry present in the Euler equations. It has been shown that the analysis and the results are entirely applicable to the multi-point statistical correlations of arbitrary order. The analysis has revealed new *similarity solutions* (*scaling laws*) which are manifestations of particular broken symmetries admitted by the original system.

The analysis firstly recovers the classical, *diffusion-like, heat-equation-like*, solution in the case that all the symmetries are valid. This similarity solution is characterized by a power-law decay of the turbulent kinetic energy with the distance from the forcing plane, x^{-n}, in the limit $t \to \infty$ and the linear growth of the integral length scales with time. The propagation of the TNTI has been shown to take place according to

$$H\left(t\right) \sim \left[\left(t - t_0\right)/\tau\right]^m \tag{1}$$

where $H\left(t\right)$ is the distance of the TNTI from the forcing plane, τ is a timescale and t_0 is a temporal virtual origin (Hopfinger et al., 1982).

The second similarity solution, the *decelerating diffusion-wave* solution, is obtained by considering the symmetry breaking of scaling of space. The turbulent kinetic energy now exhibits an exponential decay with the distance from the grid, $\exp\left(-x\right)$, in the steady state limit and the integral length scales remain constant in time. The TNTI propagates according to

$$H\left(t\right) \sim \ln\left[\left(t - t_0\right)/\tau\right] \tag{2}$$

Similar theoretical and experimental results have been obtained recently albeit in the setting of isotropic turbulence. In the experiments utilizing multiscale, fractal grids in a wind tunnel to create an isotropic turbulent field, Hurst and Vassilicos (2007) have discovered regions with an exponential decay of turbulence and constant integral length scales. George and Wang (2009) have analyzed the similarity solutions to the energy equation in the spectral space and recovered an exponential temporal decay of turbulence when the (integral) length scales are kept constant.

An additional similarity solution is obtained by introducing constant system rotation with the axis perpendicular to the forcing plane, and thereby breaking the symmetry of scaling of time. The turbulent kinetic energy now decays according to x^{-2} and the TNTI ceases to propagate beyond a certain distance which is the asymptote to the function governing the position of the TNTI

$$H\left(t\right) \sim \exp\left[-\left(t - t_0\right)/\tau\right] \tag{3}$$

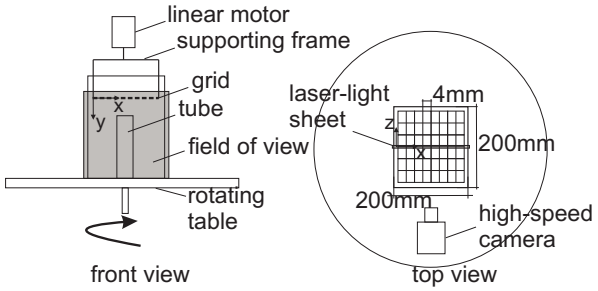

Figure 1: Sketch of the experimental setup

This case has been investigated mainly in the steady state limit, and several characteristics of the turbulent field have been emphasized, e.g. the quasi-two-dimensionalization with distance to the grid, the appearance of coherent vortices which are alligned with the axis of rotation, the interaction of inertial waves and turbulent motions, the modulation of the energy spectrum by rotation, etc (e.g. Dickinson and Long 1975, Hopfinger et al., 1978, Godeferd and Lollini, 1999). The investigations of the unsteady problem of tracking the TNTI has revealed difficulties in balancing proper TNTI propagation with the effects of rapid quasi-two-dimensionalization and its treatment is out of scope of the present paper.

EXPERIMENTS

For the measurements we used the experimental setup described in Holzner et al. (2006). A screen of squared bars (diameter $d = 1$mm, mesh-size $M = 4$mm) is installed near the upper edge of a water filled glass tank with dimensions 200 x 200 x 300mm^3. The grid is connected to a linear motor, which drives the vertical oscillation on a supporting frame connected to the grid through four rods of 4mm in diameter. The motor, operated in a closed loop with feedback from a linear encoder, runs at a frequency of $f = 9$Hz and an stroke amplitude $S = 8$mm for all the experiments. The PIV experiments were conducted by using a high-speed camera (Photron Ultima APX, 1,024x1,024 pixels) at a frame rate of 50 Hz. The beam of a continuous 25 Watt Ar-Ion laser is expanded through a cylindrical lens and forms a planar laser sheet about 1 mm thick, which passes vertically through the mid-plane of the tank. Polystyrol particles with a mean diameter of 40 μm were used as passive flow tracers. The density of the fluid was matched with the density of the tracers of 1.05 g/cm^3 utilizing sodium cloride. Additional visualisation experiments using Pearlescence, which are plate-like particles that align with shear, were carried out for a better visualization of the flow.

Detection of the TNTI position

The propagation of the TNTI is analysed by using the level-based technique described in Holzner et al. (2006). This method uses a fixed out-of-plane vorticity threshold to distinguish between turbulent and calm ambient fluid. The threshold is calculated by multiplying the noise level of the out-of-plane verticity by a factor of four. Holzner et al.(2006) derived this factor by comparison with the results of dye measurements among others. The propagation of the TNTI estimated from the Perlescence experiments also qualitatively confirms the chosen threshold. For each time instant and for each position x, the position of the TNTI is the lowest point $y^*(x,t)$ at which the magnitude of

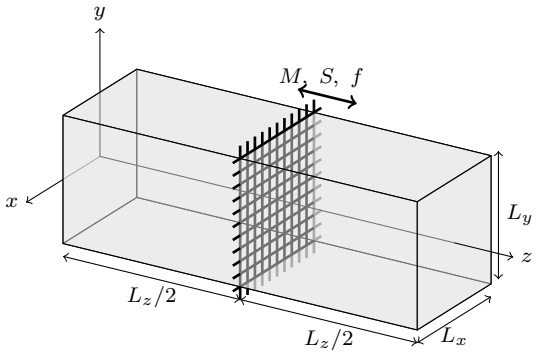

Figure 2: Sketch of the computational domain with position of turbulence sources

the out-of-plane vorticity exceeds the threshold. The instantanious mean position of the TNTI is the horizontal average over the point detected by the method. Similar methods were used by Westerweel et al. (2002) (see also Westerweel et al. (2005) and references therein).

SIMULATIONS

Numerical experiments in the LES framework have been performed, aiming to assess conformance of the methodology to the above outlined constraints of the statistical quantities of turbulence. The symmetry groups of the Navier-Stokes equations are equally admittable by all the evolution equations of the statistical quantities of turbulence which are derived from them using the operations of averaging or convolution filtering (Oberlack, 1997). Consequently, any closure relationship used in the statistical equations should also conform to the constraints imposed by the symmetry groups.

In the present LES work the unknown *filtered* velocity field is governed by the following equations in Cartesian tensor notation

$$\frac{\partial u_i}{\partial t} + \frac{\partial}{\partial x_j}\left(u_i u_j\right) = -\frac{\partial p}{\partial x_i} + \frac{\partial}{\partial x_j}\left(S_{ij} - \tau_{ij}\right) + f_i \qquad (4)$$

$$\frac{\partial u_i}{\partial x_i} = 0 \qquad (5)$$

Here, u_i are the components of the filtered velocity field, p is the effective pressure field, f_i is the volumetric force, $S_{ij} \equiv \left(\partial_j u_i + \partial_i u_j\right)/2$ is the rate of strain tensor and $\tau_{ij} \equiv \overline{\tilde{u}_i \tilde{u}_j} - u_i u_j$ (where $\overline{\tilde{u}_i} \equiv u_i$) is the tensor arising from the filtering of the nonlinear term in the Navier-Stokes equations. Formally, additional terms arise in the equations governing evolution of the filtered velocity field, such as the results of non-commutativity of the differential and filtering operators, but these are usually represented within a model for the unknown tensor τ_{ij} or can be avoided by using commutative filters and/or discretisation formulae.

The localized dynamic version of the Smagorinsky model was used to approximate the effects of the unresolved motions. In their analysis of several sub-grid scale modelling approaches Razafindralandy et al. (2007) concluded that this particular form of closure theoretically satisfies all the symmetry constraints of the Navier-Stokes equations. In the framework of eddy-viscosity models the deviatoric part of the sub-grid scale tensor is taken to be localy proportional to the resolved rate of strain

$$\tau_{ij} = 2\nu_{sgs}S_{ij} + \frac{2}{3}k\delta_{ij} \tag{6}$$

where $k = \tau_{ii}/2$. This modelling approach parametrizes the sub-grid stress with k and ν_{sgs} (Fureby et al., 1997) according to

$$k = c_I\Delta^2\|S_{ij}\|^2 \tag{7}$$

$$\nu_{sgs} = c_D\Delta^2\|S_{ij}\| \tag{8}$$

Here, the unknown parameters c_I and c_D are dynamically determined by utilizing scale-similarity of filtered quantities at different filtering levels and solving an overdetermined system of equations in the least-square sense (Germano et al, 1993).

Computational method

The simulations have been performed utilizing OpenFOAM computational continuum mechanics library. The library implements the finite volume method (FVM) of discretizing partial differential equations. Computational grids are allowed to consist of general polyhedra. Second order discretization is employed in space and time, employing the standard central differencing in space and backward difference scheme in time. Table 1 summarizes the numerical parameters used in the present work.

The experimental turbulence tank has been represented as a computational box, Fig. 2, ($L_x,\ L_y,\ L_z$) with periodic boundary conditions imposed on boundary planes perpendicular to the forcing plane. At the boundaries parallel to the forcing plane several boundary conditions have been compared - symmetry plane, zero-gradient and the advective (which imposes a value of a variable by solving local advection equation $Du_i/Dt = 0$) boundary condition. The different boundary conditions have been found to produce only minor changes in the solution when the distance of the boundary to the forcing plane is appropriately chosen.

Forcing

The volumetric force is given by the following expression (Godeferd and Lollini, 1999)

$$f_z\left(x, y, z_g, t\right) = \frac{(2\pi f)^2 S}{2}\left[\delta_{1i}\cos\left(\frac{2\pi}{M}x\right)\cos\left(\frac{2\pi}{M}y\right)\sin\left(2\pi ft\right) + \beta_i\right] \tag{9}$$

The above formulation features parameters of the oscillating grid used in the experiments, which makes it possible to compare the outcomes of the two investigations and β_i is the uniformly distributed random number in interval $[-0.25, 0.25]$.

These parameters are used to determine the Reynolds number of the system as

$$Re = \frac{fS^2}{\nu} = 576 \tag{10}$$

The analytical results assume a constant level of energy at the forcing plane, and the volumetric force should mimic this behaviour as well. Figure 3 shows the signal of the maximum velocity within the domain normalized with the mean value of the statistically steady part. It can be seen that, besides the initial transient, the energy in the forcing region remains to a good approximation constant. Spectral

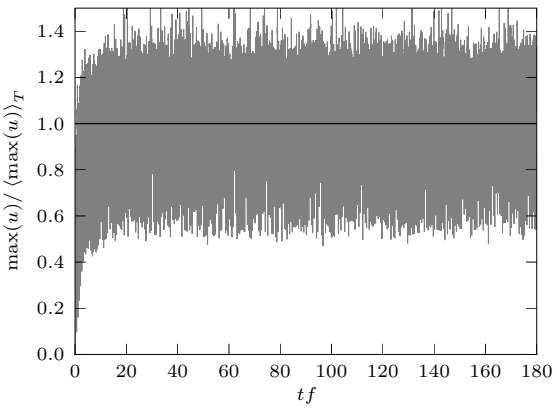

Figure 3: An example of behavior of the maximal kinetic energy within the domain ($\langle\cdot\rangle_T$ denotes time averaging, E_k is the kinetic energy)

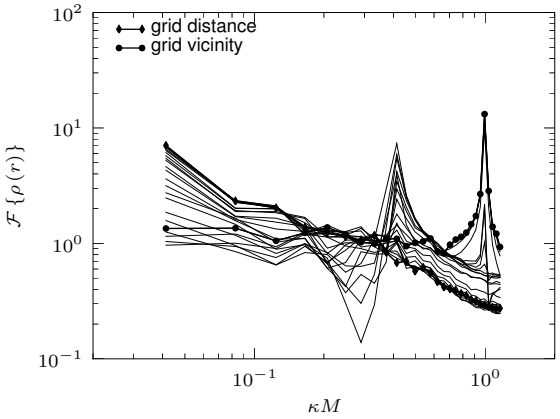

Figure 4: Fourier transform of the autocorrelation coefficient (κ denotes the wavenumber)

Table 1: Summary of the simulation domains

Name	$N_x \times N_y \times N_z$	$L_x/M \times L_y/M \times L_z/M$
fLES1	$20 \times 120 \times 20$	$25 \times 150 \times 25$
fLES2	$40 \times 240 \times 40$	$25 \times 150 \times 25$
fLES3	$40 \times 120 \times 40$	$50 \times 150 \times 50$
fLES4	$60 \times 360 \times 60$	$25 \times 150 \times 25$
cLES1	$20 \times 600 \times 20$	$2.5 \times 150 \times 2.5$
cLES2	$30 \times 450 \times 30$	$2.5 \times 75 \times 2.5$

content of the autocorrelation coefficient, Fig. 4, shows that the energy containing scales correspond to the grid spacing M in the forcing region. As the distance to the forcing region increases the energy gets transfered to the large scales, signifying merger of initial turbulent structures.

As the rate of energy input per unit mass, $\langle f_i u_i\rangle$, is proportional to the computational cell volume withing FVM, forcing has been implemented in such a manner to ensure the approximate equivalence of the forcing region for different grid resolutions by keeping the depth of the forced volume proportional to the grid stroke S.

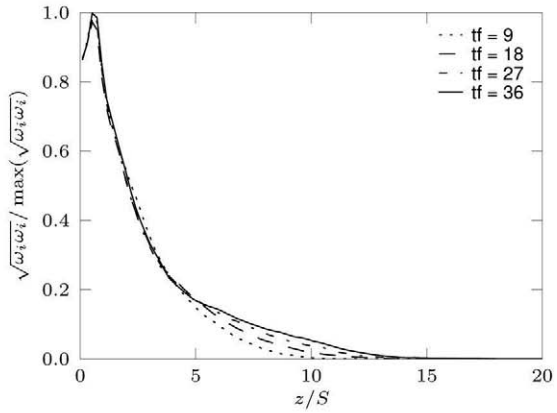

Figure 5: Vorticity magnitude profiles ($\omega_i = \epsilon_{ijk}\partial_j u_k$)

Detection of the TNTI position

The propagation of the TNTI and the entrainment process are connected with the small-scale "nibbling" motions in its vicinity. Qualitatively, the mechanisims prevalent in this region take place on spatial scales which are modelled in LES. Therefore, to ascertain the position of the TNTI from LES data poses several ambiguities. The resolved LES vorticity field is a quantity dependant on the grid size, i.e. the magnitude of the resolved vorticity is inversely proportional to the grid size. The front position has been detected by setting a fixed threshold on the vorticity profile which is calculated as an average of the vorticity magnitude in statistically homogeneous planes and statistically symmetric (with respect to the forcing region) layers of cells.

Fig. 5 shows the averaged vorticity profiles with the distance from the grid. (for comparison to DNS see the paper of Khujadze and Oberlack elsewhere in these proceedings). The growth of the turbulent region is apparent in both figures. The absence of the clear strong vorticity gradient in direction of the propagation in Fig. 5 further elucidates the above mentioned difficulty in calculating the position of the TNTI.

RESULTS

In Fig. 6, an example of behaviour of the autocorrelation coefficient, $\rho_{ij}(r,x) \equiv R_{ij}/(R_{ij}|_{r=0})$, of velocity components perpendicular to the forcing plane is plotted for the case of free diffusion. The separation r lies within the statistically homogeneous planes. As indicated from the Fig. 4, velocities are strongly correlated over distances of the order M in the vicinity of the forcing. The separation over which the velocities are correlated increases with the distance from the grid thereby indicating growth of the integral length scales.

In Figures 7 and 8 snapshots of vorticity magnitude are shown. Experimental contours show threshold of the out-of-plane vorticity magnitude. The LES snapshots are taken from the midplane of the computational domain perpendicular to the forcing plane. Qualitatively, the multiscale contortion of the interface may be observed. The confined case shows no apparent propagation which is consistent with the expected slow logarithmic growth.

Propagation of the TNTI in the case of free diffusion is presented in Fig. 9. The power-law-like lines presented show qualitative agreement of both experiments and simulations with the analytical predictions.

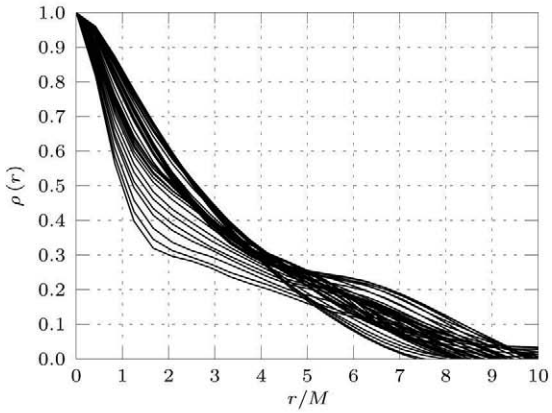

(a)

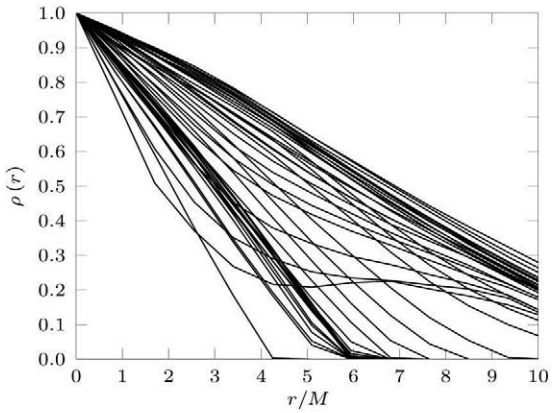

(b)

Figure 6: Autocorrelation coefficient of the velocity components perpendicular to the forcing (a) simulations, (b) experiments

Similarly, in the case of turbulent diffusion with confined growth of length scales qualitative agreement is obtained between both sets of data and the predictions, Fig. 10 Turbulence propagates extremely slowly relative to the unconfined case and follows the logarithmic trend.

The discrepancy in the TNTI apparent from the data may be attributed to several causes. In the experiments, the vicinity of the side walls, and as the front propagates of the tank bottom wall influence the behaviour at later stages of propagation. Causes of disagreements among the simulation data are to be traced to general complexity in establishing clear criteria in setting the vorticity threshold in response to computational grid refinement/unrefinement. Additionaly, due to the random component of the body force employed, changes in numerical resolution cause aliasing in the actual forcing wavenumber which brings further uncertainty.

CONCLUSIONS AND OUTLOOK

The present paper investigated two similarity solutions to the problem of turbulent diffusion from a planar source of energy into an infinite body of fluid. The results obtained indicate qualitative agreement between the mathematical

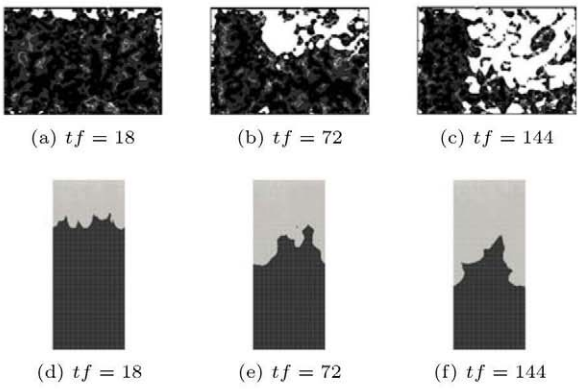

(a) $tf = 18$ (b) $tf = 72$ (c) $tf = 144$

(d) $tf = 18$ (e) $tf = 72$ (f) $tf = 144$

Figure 7: Snapshots of instantaneous vorticity in the case of free diffusion (a), (b), (c) experiments and (c), (d), (e) simulations at dimensionless times tf

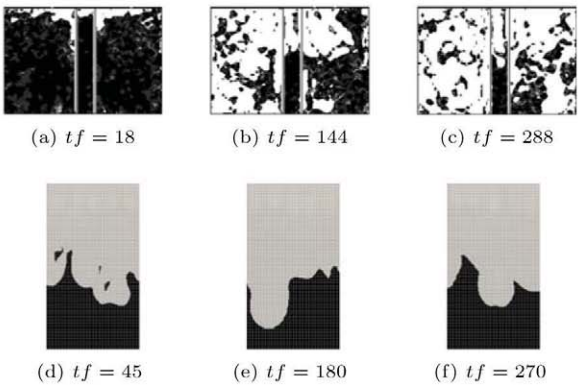

(a) $tf = 18$ (b) $tf = 144$ (c) $tf = 288$

(d) $tf = 45$ (e) $tf = 180$ (f) $tf = 270$

Figure 8: Snapshots of instantaneous vorticity in the case of confined diffusion (a), (b), (c) experiments and (c), (d), (e) simulations at dimensionless times tf

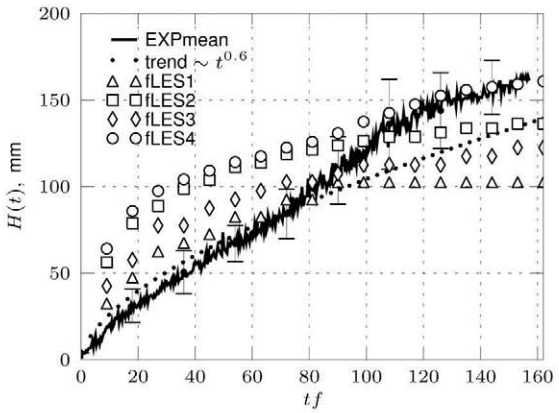

(a)

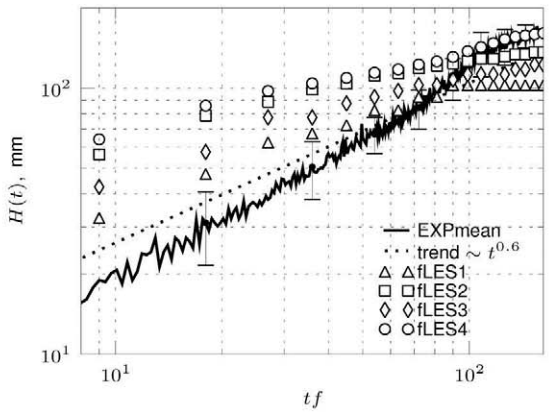

(b)

Figure 9: Behavior of the TNTI for the case of free diffusion

predictions and experimental and numerical data. Particularly, power-law propagation of the TNTI has been recovered in the classical case of shearless turbulent diffusion and logarithmic trend is observed in the case when confinement to the flow inhibits growth of the integral length scales of turbulence. The third similarity solution obtained analyticaly (with rotation) will be the subject of further scrutinization.

Acknowledgements

Financial support of the Deutsche Forschungsgemeinschaft (DFG) through the grant "Research Group on Turbulent Diffusion" for E. Sirbubalo and M. Kinzel is gratefully acknowledged.

REFERENCES

Dickinson S. C., and Long R. R., 1978, "Laboratory study of the growth of a turbulent layer of fluid", *Physics of Fluids*, No. 21, pp. 1968-1701

Fureby C., Tabor G., Weller H., and Gosman A. D., 1997, "A comparative study of subgrid scale models in homogeneous isotropic turbulence", *Physics of Fluids*, No. 9, pp. 1416-1429.

George W. K., and Wang H., 2009, "The exponential decay of homogeneous turbulence", *Physics of Fluids*, No. 21, pp. 1-7.

Germano M., Piomelli U., Moin P., and Cabot W. H, 1991, "A dynamic subgrid-scale eddy viscosity model", *Physics of Fluids A*, Vol. 3, No. 7, pp. 1760-1765

Godeferd F. S., and Lollini L., 1999, "Direct numerical simulation of turbulence with confinement and rotation", *Journal of Fluid Mechanics*, No. 393, pp. 257-308.

Holzner M., Liberzon A., Guala M., Tsinober A., and Kinzelbach W., 2006, "Generalized detection of a turbulent front generated by an oscillating grid", *Experiments in Fluids*, Vol. 41, pp. 711-719.

Holzner M., Lüthi B., Kinzelbach W., Liberzon A., Nikitin N., Guala M., and Tsinober A., 2007, "Study on the mechanism of turbulent entrainment through 3D-PTV and DNS", *Proceedings, Fifth International Symposium on Turbulence and Shear Flow Phenomena*, R. Friedrich et al., ed., Vol. 1, pp. 125-130.

Hopfinger E. J., Browand F. K., and Gagne Y., 1982, "Turbulence and waves in a rotating tank", *Journal of Fluid Mechanics*, No. 195, pp. 505-534

Hurst D., and Vassilicos J. C., 2007, "Scalings and decay of fractal generated turbulence", *Physics of Fluids*, No. 19, pp. 1-31.

Kinzel M., Holzner M., Lüthi B., Tropea C., Kinzelbach W., and Oberlack M., 2008, "Scaling laws of turbulent diffusion - an experimental validation", *Proceedings, 14th International Symposium on Applications of Laser Tech-*

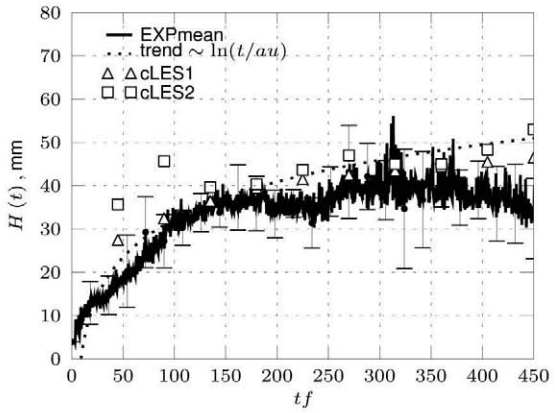

(a)

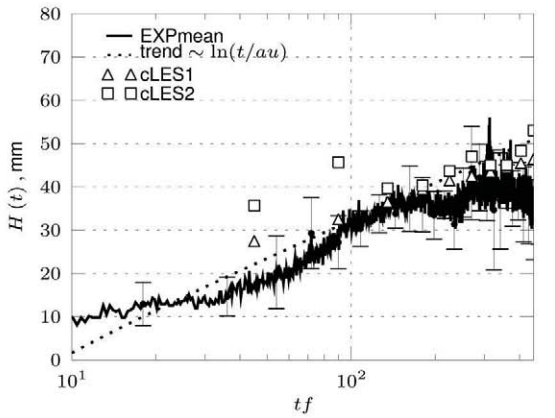

(b)

Figure 10: Behavior of the TNTI for the case of confined difusion

niques to Fluid Mechanics.

Khujadze G., and Oberlack M., 2009, "DNS of vibrating grid turbulence", Proc. *6th Int. Symposium on Turbulence and Shear Flow Phenomena - TSFP6*, Seoul National University, Seoul, Korea, June 22-24

Lele. S. K., 1985, "A consistency condition for Reynolds stress closures", *Physics of Fluids*, No. 28, pp. 64-68

Oberlack M., 1997, "Invariant modelling in large-eddy simulation of turbulence", *Annual Research Briefs, Center for Turbulence Research*, pp. 3-22

Oberlack M., and Guenther S., 2003, "Shear-free turbulent diffusion, classical and new scaling laws", *Fluid Dynamics Research*, Vol. 33, pp. 453-476.

Razafindralandy D., Hamdouni A., and Oberlack M., 2007, "New turbulence models preserving symmetries", *Proceedings, Fifth International Symposium on Turbulence and Shear Flow Phenomena*, R. Friedrich et al., ed., Vol. 1, pp. 315-320.

Weller H. G., Tabor G., Jasak H., and Fureby C., 1998, "A tensorial approach to computational continuum mechanics using object-oriented techniques", *Computers in Physics*, Vol. 12, pp. 620-631.

Westerweel J., Fukushima C., Pedersen J. M., and Hunt J., 2005, "Mechanics of the turbulent-nonturbulent interface of a jet", *Physical Review Letters*, Vol. 95: 174501

Westerweel J., Hoffmann T., Fukushima C., and Hunt J., 2002, "The turbulent/non-turbulent interface at the outer boundary of a self similar jet", *Experiments in Fluids*, Vol. 33, pp. 873-878